Hindawi
International Journal of Energy Research
Volume 2024, Article ID 1667398, 12 pages
https://doi.org/10.1155/2024/1667398

WILEY | Hindawi

Research Article

Electrochemical-Thermal-Mechanical Coupling Analysis of Lithium-Ion Batteries under Fast Charging

Yaohong Suo,[1,2] **Qiongnan Jia**,[2] **Mingju Lin**,[1] **and Zhongyang Chen**[2]

[1]*School of Mechanical Engineering and Automation, Fuzhou University, Fuzhou, Fujian 350108, China*
[2]*School of Advanced Manufacturing/School of Ocean, Fuzhou University, Jinjiang, Fujian 350108, China*

Correspondence should be addressed to Yaohong Suo; yaohongsuo@126.com

Received 22 October 2023; Revised 1 December 2023; Accepted 19 March 2024; Published 12 April 2024

Academic Editor: Denis Osinkin

Thermal runaway and volume expansion caused by temperature rise under fast charging of lithium-ion batteries (LIBs) are the major reasons of battery explosion and cycle performance degradation. In this work, considering the radiation heat transfer on the battery surface, an electrochemical-thermal-mechanical coupling model of cylindrical LIBs under fast charging (state of charge (SOC) ≤80%) is developed in order to investigate the distributions of the temperature and stress. Then, choosing 18650 LIBs as the object, the charge efficiency, temperature, and stress distributions are compared between fast charging and galvanostatic operation under SOC≤80%, respectively. Finally, the influences of the thickness, particle radius, the maximum lithium-ion concentration of the cathode, and initial electrolyte concentration on the temperature, radial stress, and hoop stress of LIB during charge are explored, respectively. Numerical results show that fast charging improves 20.8% of the charge efficiency. Increasing the cathodic thickness and decreasing the cathodic maximum lithium-ion concentration or initial electrolyte concentration can reduce the temperature of LIB during the charge. The results of this work will provide some reference value for the design of LIBs under fast charging.

1. Introduction

Lithium-ion batteries (LIBs) are widely utilized in portable devices, energy storage systems, and electric vehicles because of their low self-discharge rate, long cycle life, low energy density, small size, and no memory effect [1]. Nowadays, the pursuit of higher charge efficiency is one of the research focuses of LIBs. However, in this process, the safety problem of LIBs becomes more prominent. For example, the temperature rise of LIBs due to heat generation during the charge may lead to thermal runaway or battery explosion. In addition, the bulge and deformation of the battery due to the temperature rise results in the degradation of cycle performance, material failure, and even fracture [2–4]. Therefore, in order to ensure the safety of LIBs under fast charging and provide some references for the design of LIBs, it is necessary to analyze the distributions of the temperature and stress of LIBs during fast charging.

At present, the thermal generation characteristics of LIBs have been paid more attention [5–8]. For example, Thakur et al. [9] discussed the thermal issue during fast charging rate and its effect on performance degradation and thermal runaway. Moreover, thermal management systems for fast charging were reviewed. Wu et al. [10] developed an electrochemical-thermal model to access the heat generation of cylindrical LIBs with the discharge rates and N/P ratio. Tang et al. [11] used a one-dimensional electrochemical-thermal coupling model to discuss the heat generation characteristics of LIBs during charge and discharge cycles. Srinivasan and Wang [12] developed a two-dimensional electrochemical-thermal coupling model for $LiMn_2O_4$ to study the variation of resistance with state of charge (SOC) at different discharge currents and the proportion of reversible heat, irreversible heat, and ohmic heat in the heat generation of the battery. Xu et al. [13] analyzed the effect of the two-stage fast charging process on the temperature of cylindrical batteries. Zhou et al. [14] proposed a distributed thermal monitoring framework to investigate the global temperature distribution of the pouch cell. Pegel et al. [15] studied the temperature characteristics of lithium-ion

batteries under galvanostatic operation by an electrochemical-thermal coupling model, focusing on the heat generation ratio of different regions and the heat generation of positive and negative electrodes. Mei et al. [16] analyzed the effects of electrode parameters on the electrochemical performance and thermal characteristics of LIBs by an electrochemical-thermal coupling model. Li et al. [17] investigated the effects of discharge multiplicity and ambient temperature on the electrochemical and thermal characteristics of the battery. These above researches had analyzed the heat generation and temperature of lithium-ion batteries. However, the influence of the deformation on the temperature is not taken into account under fast charging.

During the charge and discharge, the thermal expansion due to the temperature rise can cause electrode deformation and capacity decay. Therefore, thermal stress induced by temperature rise should be analyzed. Jin et al. [18] calculated the distributions of temperature and stress in a square soft pack LIB and found that the stress varied with the discharge rate and ambient temperature. Valentin et al. [19] evaluated the thermomechanical behavior of the multilayer section of 18650 lithium-ion cells during discharge and found that the difference between the mechanical material properties led to specific stresses at the multiple interfaces. Zhang et al. [20] proposed a thermomechanical coupled structural model of LIBs to discuss the influence of mechanical deformation on electrochemical properties. Suo and Liu [21] developed a thermal-mechanical coupled model of LIBs with a constant heat source to analyze the distributions of temperature and stress. You et al. [22] calculated the static stresses of lithium bag batteries at different charge and discharge currents by a coupled electrothermal-mechanical model. Tian and Xiao [23] simulated the temperature distribution under different ambient temperatures in a thermomechanical coupling model under the fast charging condition. These above studies analyzed the stresses in LIBs. However, most of them only considered reaction heat and ohmic heat and ignored polarization heat. In addition, their charge efficiency was lower.

Based on these above discussions, an electrochemical-thermal-mechanical coupling model of cylindrical LIBs under fast charging is developed in this work. Then, choosing 18650 LIBs as the object, the comparisons of the charging efficiency, temperature, and stress distributions between fast charging and galvanostatic operator are, respectively, made under SOC ≤ 80%. Finally, the influences of cathode thickness, cathode particle radius, maximum lithium-ion concentration of cathode, and initial electrolyte concentration on the temperature, radial stress, and hoop stress of LIBs under fast charging are discussed, respectively.

2. Mathematical Models

2.1. Electrochemical Model. The diffusion and migration of lithium-ions in the battery and the electrochemical reaction process satisfy the mass conservation, charge conservation, and electrochemical kinetic equations [24, 25], respectively. The electrochemical model [10] of LIBs is expressed by Ohm's law in the solid phase as follows:

$$-\sigma_s \frac{\partial \phi_s}{\partial x} = i_s, \tag{1}$$

with the boundary condition

$$-\sigma_s \frac{\partial \phi_s}{\partial x}\bigg|_{x=L} = \frac{I}{A}, \tag{2}$$

where σ_s is the solid phase conductivity (S/m), ϕ_s is the solid phase potential (V), x is the electrode orientation coordinate of the battery, and i_s is the electrode current density with $i_s = I/A$ in which A is the electrode plate area (m^2) and I is the current (A) of fast charging [26].

At present, the researches on various fast charging methods for LIBs are mainly based on Mas's optimal charging curve as shown in [27]. When the charge current is much higher than the optimal charge current, the gas precipitation of the battery will be increased and the polarization reaction of the battery will be aggravated, thus causing the service life to be shorten. When the charge current is lower than the optimal charge current, the charge time will be increased and the charge efficiency will be low. To reduce charge time and improve charge efficiency, the charging current must be maintained near the optimal charging curve. Obviously, galvanostatic operation is not an ideal charging pattern, and the optimal charging is hard to control the charging current. Therefore, a multistage constant current charge is the best approach to the optimal charging curve. In this work, the optimal charge curve is approximated by using a seven-stage constant current method, as shown in Figure 1. That is, the threshold of the charge capacity in every segment is, respectively, 20%, 30%, 40%, 50%, 60%, 70%, and 80%, and the corresponding charge current is, respectively, 1.28 C, 1.12 C, 0.96 C, 0.8 C, 0.66 C, 0.52 C, and 0.38 C, where C-rate is a measurement of the rate at which a battery is charged or discharged relative to its nominal capacity.

It is noticed that this charge shown in Figure 1 is called fast charging. As well known, the usual charge is galvanostatic and potentiostatic operation. But, the charge current of galvanostatic operation is much larger than that of the optimal charge curve near the end of the charge which results in lower charge efficiency. Although the optimal charge current is best, it is very difficult to operate during charge. Therefore, the seven-stage charge shown in Figure 1 is closer to the optimal charge current curve and it will shorten the charge time and improve charge efficiency.

The solid phase charge conservation equation [9] satisfies Ohm's law as follows:

$$\frac{\partial}{\partial x}\left(\sigma_s \frac{\partial \phi_s}{\partial x}\right) = j^{Li}, \tag{3}$$

with the following boundary conditions

$$\frac{\partial \phi_s}{\partial x}\bigg|_{x=L_{neg}} = \frac{\partial \phi_s}{\partial x}\bigg|_{x=L_{neg}+L_{sep}} = 0, \tag{4}$$

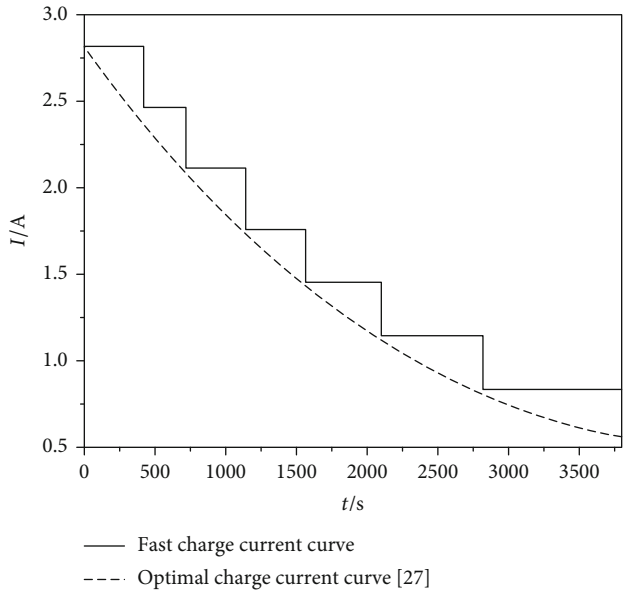

Figure 1: Fast charge current curve and optimal charge current curve.

where j^{Li} is the charge exchange current density (A/m^3) and L is the total electrode length (μm) with $L = L_{\mathrm{pos}} + L_{\mathrm{sep}} + L_{\mathrm{neg}}$ in which L_{pos}, L_{sep}, and L_{neg} are the thickness (μm) of the positive, the separator, and the negative, respectively.

The charge conservation equation of the liquid phase [10] also needs to satisfy Ohm's law as follows:

$$\frac{\partial}{\partial x}\left(\sigma_{\mathrm{e}}{}^{\mathrm{eff}}\frac{\partial \phi_{\mathrm{e}}}{\partial x}\right) = \frac{2RT}{F}\left(t_{+}^{0}-1\right)\frac{\partial}{\partial x}\left(\sigma_{\mathrm{e}}{}^{\mathrm{eff}}\frac{\partial \ln c_{\mathrm{e}}}{\partial x}\right) + j^{\mathrm{Li}}, \quad (5)$$

with the following boundary conditions

$$\left.\frac{\partial \phi_{\mathrm{e}}}{\partial x}\right|_{x=0} = \left.\frac{\partial \phi_{\mathrm{e}}}{\partial x}\right|_{x=L} = 0, \quad (6)$$

where $\sigma_{\mathrm{e}}{}^{\mathrm{eff}}$ is the effective diffusive conductivity (S/m) with $\sigma_{\mathrm{e}}{}^{\mathrm{eff}} = \sigma_{\mathrm{e}} \cdot \varepsilon_{\mathrm{e}}{}^{\beta}$ and σ_{e} and β are the liquid phase conductivity (S/m) and Brueggemann coefficient, respectively. ϕ_{e} is the liquid phase potential (V), R is the universal gas constant (J/(mol·K)), T is the temperature (K), F is the Faraday constant (=96485 C/mol), t_{+}^{0} is the lithium-ion transfer coefficient, and c_{e} is the liquid-phase lithium-ion concentration (mol/m^3).

The mass conservation equation [18] of Li-ion diffusion in the solid phase satisfies Fick's second law as follows:

$$\frac{\partial c_{\mathrm{s}}}{\partial t} = \frac{1}{r_{\mathrm{s}}{}^{2}}\frac{\partial}{\partial r_{\mathrm{s}}}\left(D_{\mathrm{s}} r_{\mathrm{s}}{}^{2}\frac{\partial c_{\mathrm{s}}}{\partial r_{\mathrm{s}}}\right). \quad (7)$$

The initial Li-ion concentration is supposed to be $c_{\mathrm{s},0}$ in the solid phase, Li-ion flux is 0 at the center of the electrode particle, and Li-ion flux at the surface is consistent with the production or consumption rate where the electrochemical reactions occur. Thus, the initial and boundary conditions are as follows:

$$\begin{aligned} c_{\mathrm{s}}|_{t=0} &= c_{\mathrm{s},0}, \\ \left.\frac{\partial c_{\mathrm{s}}}{\partial r_{\mathrm{s}}}\right|_{r_{\mathrm{s}}=0} &= 0, \\ -D_{\mathrm{s}}\left.\frac{\partial c_{\mathrm{s}}}{\partial r_{\mathrm{s}}}\right|_{r_{\mathrm{s}}=R_{\mathrm{s}}} &= \frac{j^{\mathrm{Li}}}{F}, \end{aligned} \quad (8)$$

where c_{s} is the solid phase lithium-ion concentration (mol/m^3), t is the time (s), r_{s} is the radial coordinate along the active material particles, D_{s} is the solid phase lithium-ion diffusion coefficient (m^2/s), and R_{s} is the spherical particle radius (μm).

The mass conservation equation [18] of Li-ion diffusion in the liquid phase is expressed as

$$\varepsilon_{\mathrm{e}}\frac{\partial c_{\mathrm{e}}}{\partial t} = \frac{\partial}{\partial x}\left(D_{\mathrm{e}}\frac{\partial c_{\mathrm{e}}}{\partial x}\right) + \frac{1-t_{+}^{0}}{F}j^{\mathrm{Li}}, \quad (9)$$

with the following initial and boundary conditions:

$$\begin{aligned} c_{\mathrm{e}}|_{t=0} &= c_{\mathrm{e},0}, \\ \left.\frac{\partial c_{\mathrm{e}}}{\partial x}\right|_{x=0} &= \left.\frac{\partial c_{\mathrm{e}}}{\partial x}\right|_{x=L} = 0, \end{aligned} \quad (10)$$

where ε_{e} is the volume fraction of the liquid phase and D_{e} is the diffusion coefficient (m^2/s) of lithium-ions in the liquid phase.

The following Bulter-Volmer equation [18] describes the electrochemical reaction at the surface of electrode particles:

$$\begin{aligned} j^{\mathrm{Li}} &= i_0\left[\exp\left(\frac{\alpha_a F}{RT}\eta\right) - \exp\left(-\frac{\alpha_c F}{RT}\eta\right)\right], \\ i_0 &= k_0 c_{\mathrm{e}}^{\alpha_a}\left(c_{\mathrm{s,max}} - c_{\mathrm{s,e}}\right)^{\alpha_a}\left(c_{\mathrm{s,e}}\right)^{\alpha_c}, \end{aligned} \quad (11)$$

with its overpotential of intercalation reaction

$$\eta = \phi_{\mathrm{s}} - \phi_{\mathrm{e}} - E_{\mathrm{eq}}, \quad (12)$$

where α_{a} is the anodic transfer coefficient, α_{c} is the cathodic transfer coefficient, k_0 is the reaction rate constant (m/s), $c_{\mathrm{s,max}}$ is the maximum lithium-ion concentration (mol/m^3), $c_{\mathrm{s,e}}$ is the lithium-ion concentration on the surface of the active material particles (mol/m^3), η is the surface overpotential (V), and E_{eq} is the open equilibrium potential (V).

The total heat generation Q (W/m^3) of the battery contains reaction heat Q_{e} (W/m^3), ohmic heat Q_{o} (W/m^3), and polarization heat Q_{p} (W/m^3). That is,

$$
\begin{aligned}
Q &= Q_e + Q_o + Q_p,\\
Q_e &= j^{Li}\frac{dE_{eq}}{dT},\\
Q_o &= -i_s \cdot \nabla\phi_s - i_e \cdot \nabla\phi_e,\\
Q_p &= j^{Li}\eta,
\end{aligned}
\tag{13}
$$

where dE_{eq}/dT is the entropy heat coefficient [25]. Notice that the current is fast charging current in the electrochemical model.

2.2. Thermal Model. For simplification, the heat transfer during the charge [28] is assumed as follows:

(1) Heat transfer occurs only in the radial direction

(2) Thermal conductivity, density, and specific heat capacity are constants

(3) The convective heat transfer appears at the surface of the battery

The heat transfer equation influenced by the deformation [29] satisfies the energy conservation as follows:

$$
k\left(\frac{\partial^2 T}{\partial r^2} + \frac{1}{r}\frac{\partial T}{\partial r}\right) + Q = \rho C_e \frac{\partial T}{\partial t} + (3\lambda + 2G)\alpha T_r \frac{\partial \theta}{\partial t}, \tag{14}
$$

where k is the thermal conductivity coefficient (W/(m·K)), ρ is the battery density (kg/m^3), C_e is the average specific heat capacity (J/(kg·K)), λ and G are the Lamé constant with $\lambda = \nu E/(1+\nu)(1-2\nu)$ and $G = E/2(1+\nu)$, ν is Poisson's ratio, E is Young's modulus (GPa), α is the thermal expansion coefficient (K^{-1}), T_r is the reference temperature (K), and $\theta = \varepsilon_r + \varepsilon_\theta + \varepsilon_z$ is the volume strain in which ε_r, ε_θ, and ε_z are the radial, hoop, and axial strains, respectively. It is worth noting that the second term on the right side of Eq. (14) indicates the effect of deformation on temperature, and if this term is removed, Eq. (14) will reduce to the pure heat conduction equation.

Suppose that the initial temperature of the battery is T_0. Due to the symmetry of the cylinder, the heat flux at the center of the battery is zero during the charge, and there is a convective heat transfer between the surface of the battery and the surrounding. Thus, the initial and boundary conditions are expressed as

$$
\begin{aligned}
&T(r,t)|_{t=0} = T_0,\\
&q|_{r=0} = 0, \quad q|_{r=r_0} = h(T - T_h)|_{r=r_0} + \varepsilon_f \sigma_b \left(T^4 - T_h^4\right)\big|_{r=r_0},
\end{aligned}
\tag{15}
$$

where T_0, h, T_h, ε_f, and σ_b are the initial temperature (K), convective heat transfer coefficient (W/(m^2·K)), ambient temperature (K), thermal radiation coefficient, and Boltzmann constant, respectively.

2.3. Mechanical Model. The equilibrium equation [15] with the influence of temperature is expressed as

$$
\frac{\partial^2 u}{\partial r^2} + \frac{1}{r}\frac{\partial u}{\partial r} - \frac{u}{r^2} = \alpha \frac{1+\nu}{1-\nu}\frac{\partial T}{\partial r}, \tag{16}
$$

where u is the radial displacement.

Suppose that the deformation of LIB is small and the stress state is the generalized plane strain [30], the geometric equations are

$$
\varepsilon_r = \frac{\partial u}{\partial r}, \varepsilon_\theta = \frac{u}{r}, \varepsilon_z = \frac{\partial w}{\partial z} = N, \tag{17}
$$

where w is the axial displacement and N is a constant.

The stress-strain relationship affected by the temperature [31] is determined by Hooke's law as

$$
\begin{aligned}
\varepsilon_r &= \frac{1}{E}[\sigma_r - \nu(\sigma_\theta + \sigma_z)] + \alpha\Delta T,\\
\varepsilon_\theta &= \frac{1}{E}[\sigma_\theta - \nu(\sigma_r + \sigma_z)] + \alpha\Delta T,\\
\varepsilon_z &= \frac{2\int_0^R r[E\alpha\Delta T - \nu(\sigma_r + \sigma_\theta)]dr}{ER_0{}^2},
\end{aligned}
\tag{18}
$$

where σ_r, σ_θ, and σ_z are the radial, hoop, and axial stress, respectively.

Suppose that the initial displacement of the battery is zero and there is no radial stress at the surface [32]. Due to the symmetry of the cylinder and the symmetry of the stress at the surface, the displacement at the center is zero. The initial and boundary conditions can be expressed as

$$
\begin{aligned}
u(r,t)|_{t=0} &= 0,\\
u|_{r=0} &= 0,\\
\sigma_r|_{r=r_0} &= 0.
\end{aligned}
\tag{19}
$$

3. Results and Discussion

In order to investigate the change of the temperature and stress under fast charging of LIBs and the influences of some design parameters on them, 18650 LIBs with 3.7 V nominal voltage and 2.2 Ah nominal capacity are taken as the research object and numerical calculations under SOC ≤ 80% were performed in COMSOL Multiphysics software. The cathode, anode, and electrolyte of 18650 LIBs are, respectively, NMC, graphite, and $LiPF_6$, and the grid number is 10000 during the numerical simulation. The electrochemical, thermal, and mechanical model parameters [15, 25, 33–35] used in the following calculations are listed in Tables 1 and 2, respectively.

3.1. Comparisons of Temperature and Stress between Fast Charging and Galvanostatic Operation. Figure 2 describes the comparisons of surface temperature, radial stress, and hoop stress between fast charging and galvanostatic operation with $I = 1.32$ A under SOC≤80%. It is observed from Figure 2(a) that (1) the temperature rises rapidly to its peak

Table 1: Electrochemical parameters of LIBs.

Parameters	Cathode	Separator	Anode
Electrode thickness ($L_{pos}, L_{sep}, L_{neg}$) ($\mu$m)	75	25	50
Spherical particle radius (R_s) (μm)	5	—	5
Volume fraction of solid phase (ε_s)	0.513	—	0.585
Volume fraction of liquid phase (ε_e)	0.417	0.724	0.363
Initial electrolyte concentration (cl_0) (mol/m^3)	1200	1200	1200
Initial lithium-ion concentration ($c_{s,0}$) (mol/m^3)	6300	—	30938
Maximum lithium-ion concentration ($c_{s,max}$) (mol/m^3)	29000	—	31570
Solid phase conductivity (σ_s) (S/m)	100	—	100
Liquid phase conductivity (σ_e) (S/m)	0.93	0.93	0.93
Solid phase lithium-ion diffusion coefficient (D_s) (m^2/s)	5.0×10^{-13}	—	1.4×10^{-14}
Liquid phase lithium-ion diffusion coefficient (D_e) (m^2/s)	1.5×10^{-10}	1.5×10^{-10}	1.5×10^{-10}
Brueggemann coefficient (β)	1.8	1.5	2.4
Reaction rate constant (k_0) (m/s)	5×10^{-10}	—	2×10^{-11}
Anodic/cathodic transfer coefficient (α_c, α_a)	0.5	—	0.5
Lithium-ion transfer coefficient (t_+^0)	0.363	—	0.363
Electrode plate area (A) (cm^2)	1800	—	1800
Entropic coefficient (dE_{eq}/dT) (V/K)	-5×10^{-5}		-1×10^{-4}

Table 2: Thermal and mechanical parameters of LIBs.

Parameters	Symbols	Values
Battery capacity/Ah	C_0	2.2
Resistance/mΩ	R_0	0.15
Radius of the battery/mm	r_0	9
Height/mm	H	65
Initial temperature/K	T_0	298.15
Reference temperature/K	T_r	298.15
Ambient temperature/K	T_h	298.15
Thermal conductivity coefficient/(W/(m·K))	k	2.6
Density/(kg/m^3)	ρ	2722
Specific heat capacity/(J/(kg·K))	C_e	970
Young's modulus/GPa	E	75.42
Poisson ratio	ν	0.325
Thermal expansion coefficient/K^{-1}	α	1.38×10^{-5}
Convective heat transfer coefficient/(W/(m^2·K))	h	10
Thermal radiation coefficient	ε_f	0.5
Battery temperature range/°C	/	0~50 [36]
Galvanostatic current/A	/	1.32 (0.6 C) [36]

due to the larger current at the initial stage of the fast charge. Moreover, the peak is within the safe temperature range of the battery. As the charge time increases, the current of the fast charge gradually decreases which leads to the temperature dropping progressively. However, the temperature gradually increases and then approaches the steady during the whole galvanostatic operation. (2) Near the end of charge (SOC = 80%), the temperature under fast charging is lower than that under galvanostatic operation and the whole charge time under fast charging ($t = 3800$ s) is shorter than that under galvanostatic operation ($t = 4800$ s). Obviously, the fast charging improves 20.8% of the charge efficiency.

Figures 2(b) and 2(c) compare the radial and hoop stresses between fast charging and galvanostatic operation, respectively. At a certain fixed position of the battery for $t = 1100$ s, the radial and hoop stresses of the battery under fast charging are larger than those under galvanostatic operation. As the charge time increases, the radial and hoop stresses gradually decrease under fast charging while they increase under galvanostatic operation. This is due to that the high charge current leads to more heat generation rate and makes battery temperature rise rapidly, which further results in larger deformation and larger stress. As the charge continues, the deformation and stress gradually decrease because the gradually decreasing charge current under fast charging results in a lower heat generation rate and further lower temperature. However, the temperature, radial stress, and hoop stress increase under galvanostatic operation.

3.2. Influences of Different Parameters on the Temperature and Stress Distribution of LIBs

3.2.1. The Influence of Negative Electrode Thickness on the Temperature and Stress. Figure 3 depicts the influence of negative electrode thickness on the temperature and stress under fast charging. From Figure 3(a), it is observed that the temperature gradually decreases from the center to the

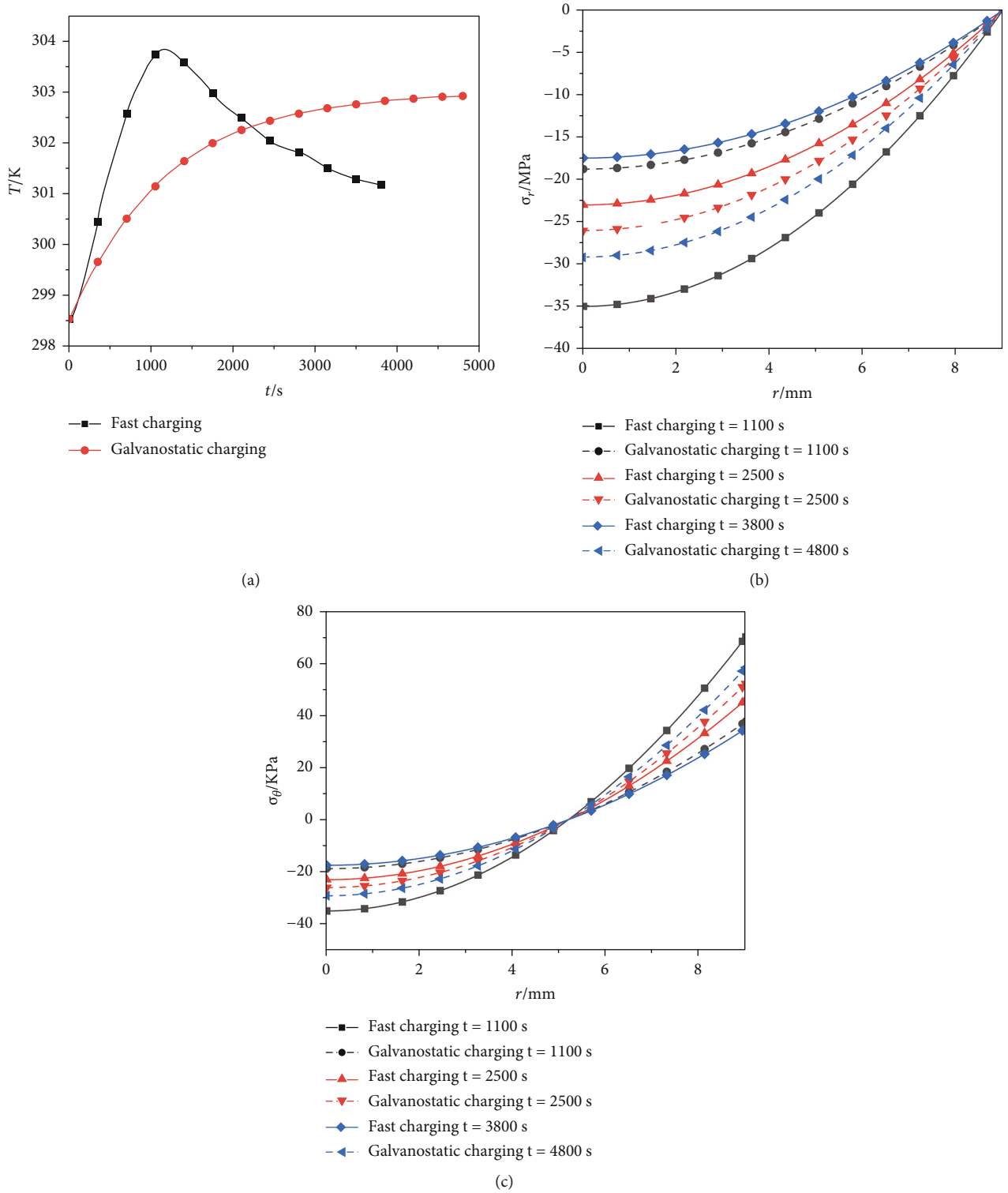

Figure 2: Comparisons of (a) surface temperature, (b) radial stress, and (c) hoop stress between fast charging and galvanostatic operation under SOC ≤ 80%.

surface, and the highest temperature appears at the center and the lowest temperature at the surface because the convective and radiative heat appears at the surface. In addition, the temperature increases with the decrease in the thickness of the negative electrode. This is because with the decrease of the thickness of the negative electrode, the impedance per length of the battery increases and thus leads to a higher heat generation rate of the battery.

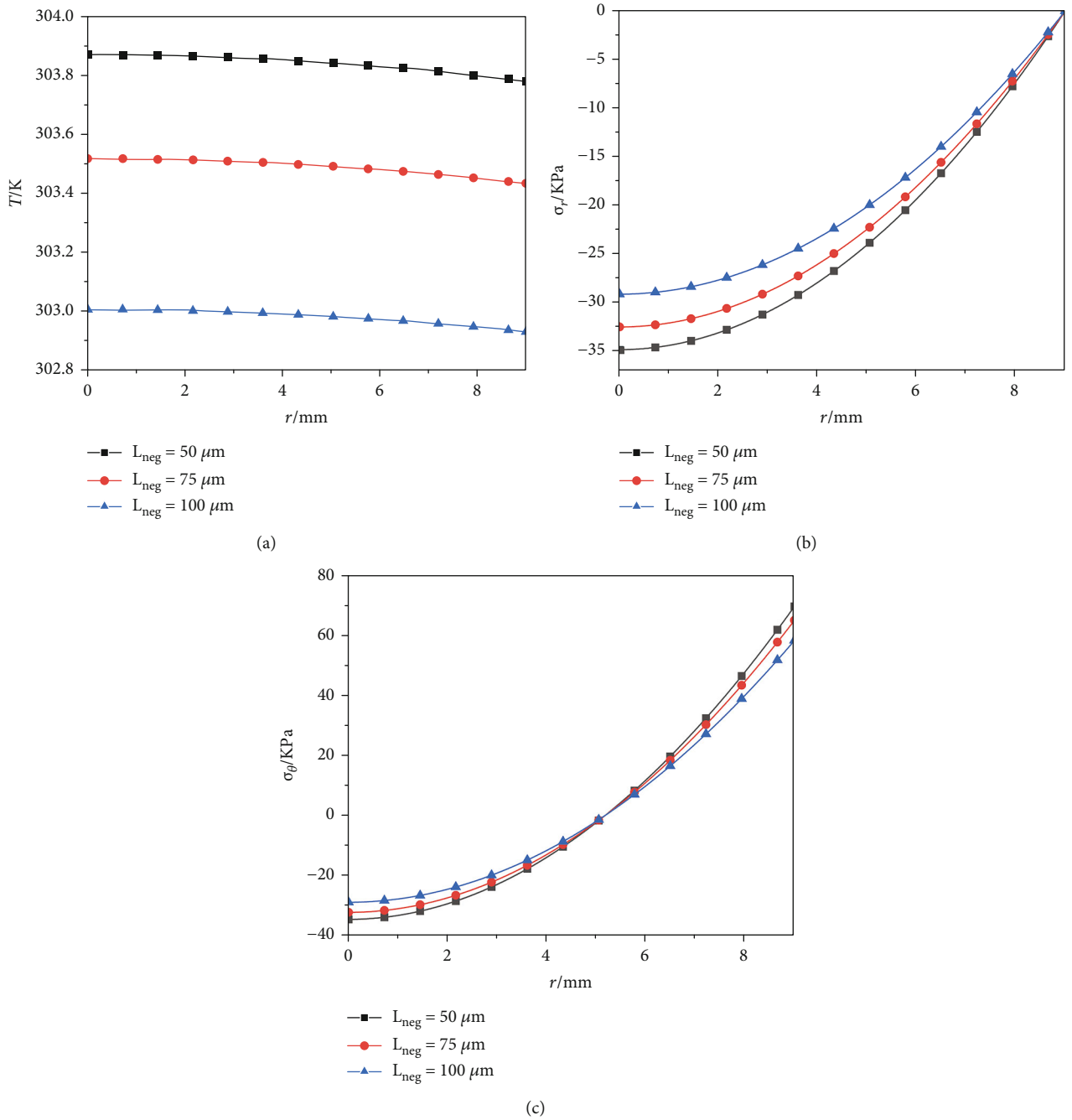

FIGURE 3: Influence of negative electrode thickness on the (a) temperature, (b) radial stress, and (c) hoop stress under fast charging at $t = 1100$ s.

The influence of negative electrode thickness on radial stress is shown in Figure 3(b). It is obviously observed that the radial direction of the battery is always in compression under fast charging and the peak of the radial stress occurs at the center. With the increase of r, the radial stress gradually decreases. At a certain fixed position of the battery, the magnitude of radial stress increases as the thickness of the negative electrode decreases. The influence of negative thickness on the hoop stress is shown in Figure 3(c). The hoop stress increases with the increase of r, and it gradually changes from the compressive stress (near the center) to the tensile one (near the surface). The peak of compressive stress appears at the center while the peak of tensile stress appears at the surface. Similarly, the smaller the negative electrode thickness is, the higher the hoop stress is. This is because the smaller thickness of the negative electrode leads to a higher temperature rise and further causes larger thermal expansion and larger stresses. Therefore, the thicker negative electrode thickness can reduce the battery temperature and avoid the failure or even destruction of the electrode material.

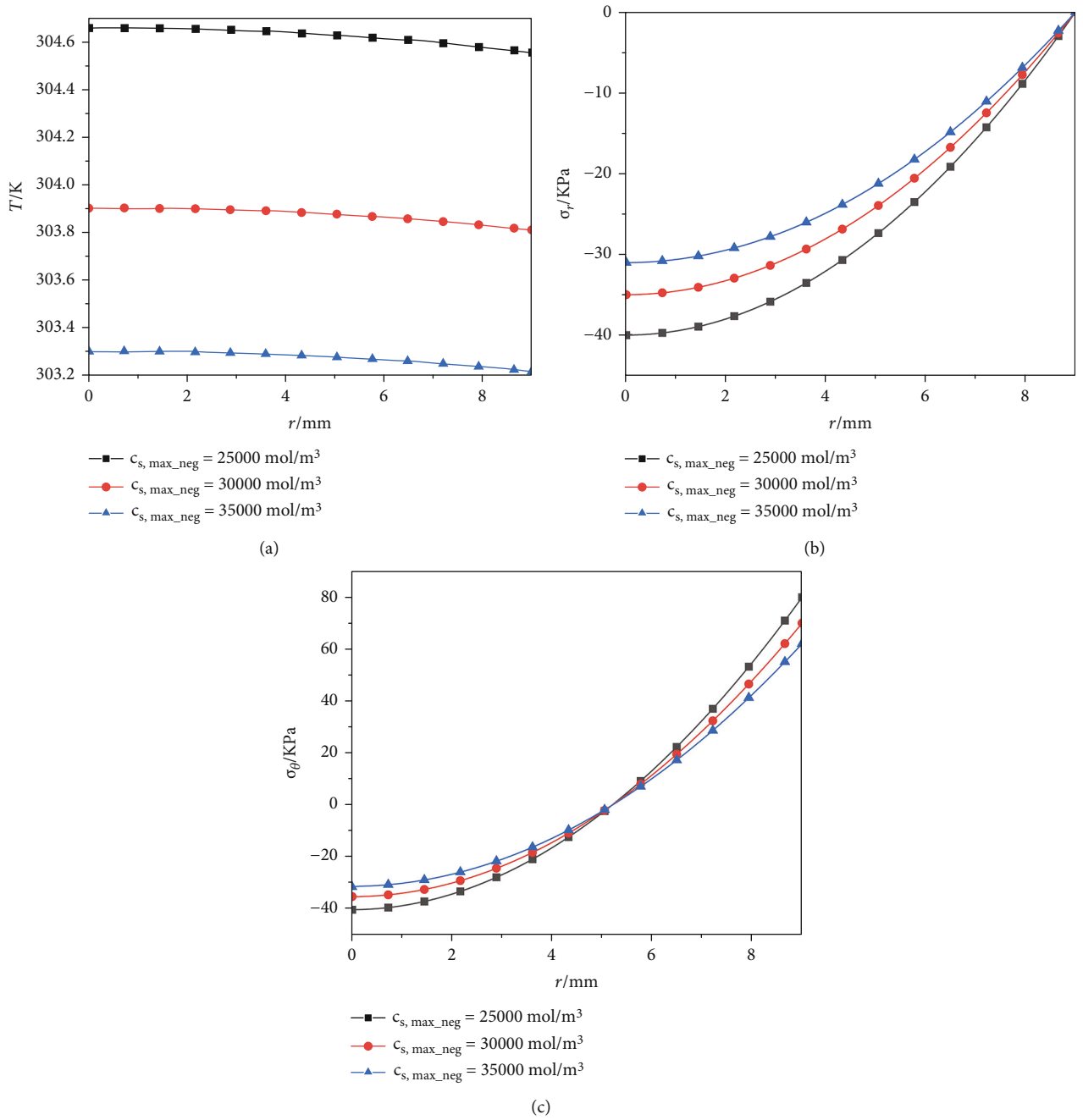

FIGURE 4: Influence of maximum lithium-ion concentration of the negative electrode on the (a) temperature, (b) radial stress, and (c) hoop stress under fast charging at $t = 1100$ s.

3.2.2. The Influence of the Maximum Lithium-Ion Concentration of the Negative Electrode on the Temperature and Stress. Figure 4 depicts the influence of the maximum lithium-ion concentration of the negative electrode on the temperature and stress under fast charging at $t = 1100$ s. From Figure 4(a), the temperature increases slightly as the maximum lithium-ion concentration of the negative electrode decreases. This phenomenon is due to that the impedance of the lithium-ion battery increases as the maximum lithium-ion concentration of the negative electrode decreases [34], which leads to an increase in the heat generation rate and temperature of the lithium-ion battery. The influences of the maximum lithium-ion concentration of the negative electrode on the radial and hoop stresses are shown in Figures 4(b) and 4(c), respectively. It can be seen that the radial and hoop stresses gradually increase with the decrease of the maximum lithium-ion concentration. This is because the higher the temperature of the battery is, the greater the thermal expansion is, which results in a larger stress. Therefore, the maximum lithium-ion concentration in the negative electrode should be increased to reduce the battery temperature and stress.

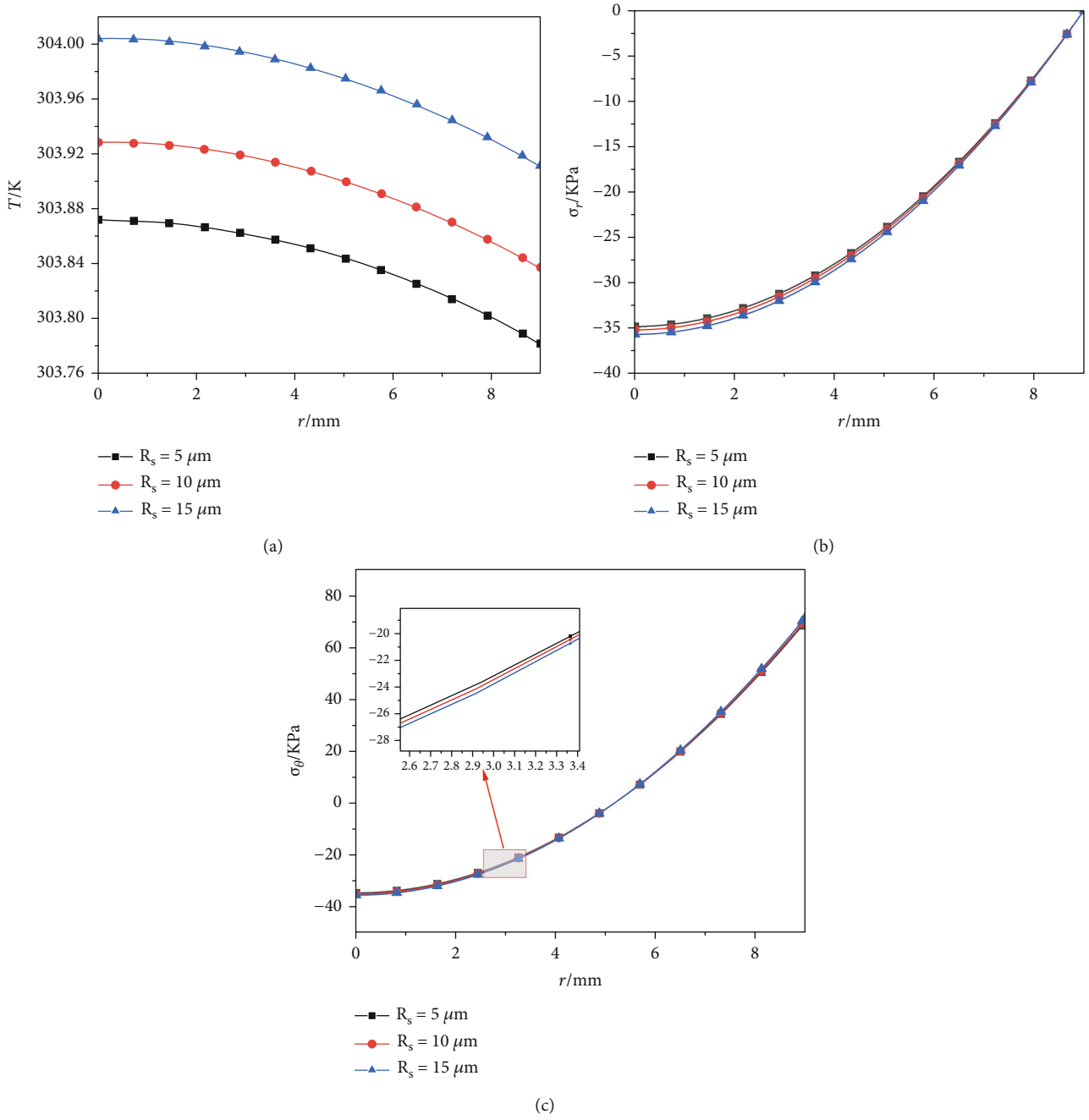

Figure 5: Influence of negative particle radius on the (a) temperature, (b) radial stress, and (c) hoop stress under fast charging at $t = 1100$ s.

3.2.3. The Influence of Negative Electrode Particle Radius on the Temperature and Stress. Figure 5 analyzes the influence of the negative particle radius on the temperature, radial, and hoop stress under fast charging. Obviously, the temperature, radial stress, and hoop stress increase slightly as the radius of the negative particle increases. This is because the larger the radius of the negative particle is, the smaller the specific surface area is, which makes the lithium-ion diffusion rate decrease and the internal resistance of the battery increase, and in turn, it can lead to the increase in the battery temperature and the increase of the radial and hoop stresses.

3.2.4. The Influence of the Initial Electrolyte Concentration on the Temperature and Stress. Figure 6 depicts the influences of the initial electrolyte concentration on the temperature and stress under fast charging. From Figure 6, it is observed that the temperature, radial stress, and hoop stress of LIBs increase with the increase of the initial electrolyte concentration. This is because, with higher electrolyte concentration, the lithium migration rate becomes quicker [34], resulting in a sharp electrochemical reaction and then leading to a higher temperature. Therefore, the initial electrolyte concentration should be appropriately reduced to decrease the temperature of LIBs.

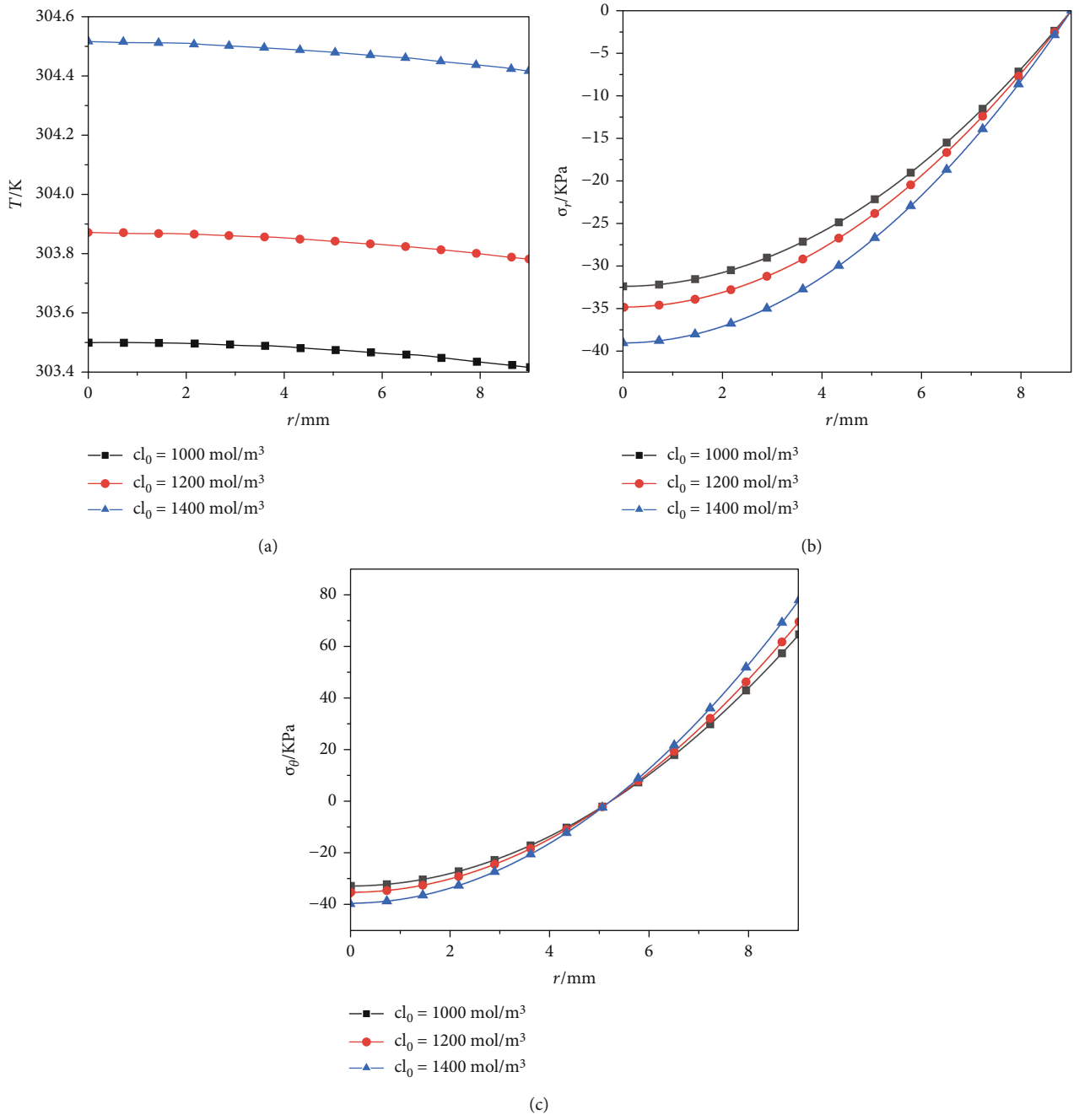

Figure 6: Influence of initial electrolyte concentration on the (a) temperature, (b) radial stress, and (c) hoop stress under fast charging at $t = 1100$ s.

4. Conclusions

In this work, a coupled electrochemical-thermal-mechanical model of a cylindrical lithium-ion battery is developed under fast charging. Then, the charging efficiency, temperature, and stress are, respectively, compared between fast charging and galvanostatic operation. The influences of some parameters on the temperature and stress of LIBs are explored during fast charging. The main conclusions are listed as follows:

(1) The seven-stage fast charging improves 20.8% of the charge efficiency

(2) Under fast charging, the temperature gradually decreases from the center to the surface, and the highest temperature occurs at the center while the maximum tensile hoop stress appears at the surface. Therefore, the hoop tensile fracture of the battery surface should be paid attention

(3) Increasing the cathodic thickness and the maximum lithium-ion concentration or decreasing the initial electrolyte salt concentration can reduce the temperature and stress of LIBs and prevent the battery from being damaged

Nomenclature

Symbols

σ_s: Solid phase conductivity
ϕ_s: Solid phase potential
I: Current
A: Electrode plate area
j^{Li}: Charge exchange current density
L: Total electrode length
L_{pos}, L_{sep}, L_{neg}: The thickness of the positive, the separator, and the negative, respectively
σ_e^{eff}: Effective diffusive conductivity
σ_e: Liquid phase conductivity
β: Brueggemann coefficient
ϕ_e: Liquid phase potential
R: Universal gas constant
T: The temperature
F: Faraday constant
t_+^0: Lithium-ion transfer coefficient
c_e: Liquid-phase lithium-ion concentration
c_s: Solid phase lithium-ion concentration
t: Time
D_s: Solid phase lithium-ion diffusion coefficient
R_s: Spherical particle radius
D_e: Liquid phase lithium-ion diffusion coefficient
k_0: Reaction rate constant
Q_e: Reaction heat
Q_o: Ohmic heat
Q_p: Polarization heat
k: Thermal conductivity coefficient
C_e: Average specific heat capacity
E: Young's modulus
T_0: Initial temperature
T_r: Reference temperature
T_h: Ambient temperature
h: Convective heat transfer coefficient
u: Radial displacement
w: Axial displacement.

Greek Letters

ε_e: Volume fraction of liquid phase
α_a: Anodic transfer coefficient
α_c: Cathodic transfer coefficient
η: Surface overpotential
ρ: Battery density
λ, G: Lamé constant
ν: Poisson's ratio
ε_r, ε_θ, ε_z: Radial, hoop, and axial strain, respectively
ε_f: Thermal radiation coefficient
σ_r, σ_θ, σ_z: Radial, hoop, and axial stress, respectively
σ_b: Boltzmann constant
β: Brueggemann coefficient.

Abbreviations

LIBs: Lithium-ion batteries
EV: Electric vehicles
SOC: State of charge.

Subscripts and Superscripts

pos: Positive
neg: Negative
sep: Separator
eff: Effective
r: Radial direction
θ: Hoop direction
z: Axial direction.

Data Availability

The data that supports the findings of this study are available from the corresponding author.

Conflicts of Interest

The authors declare that they have no conflicts of interest.

Acknowledgments

This work is supported by the National Natural Science Foundation of China (Grant No. 12272095).

References

[1] S. Panchal, M. Mathew, R. Fraser, and M. Fowler, "Electrochemical thermal modeling and experimental measurements of 18650 cylindrical lithium-ion battery during discharge cycle for an EV," *Applied Thermal Engineering*, vol. 135, pp. 123–132, 2018.

[2] A. Mukhopadhyay and B. W. Sheldon, "Deformation and stress in electrode materials for Li-ion batteries," *Progress in Materials Science*, vol. 63, pp. 58–116, 2014.

[3] T. M. Bandhauer, S. Garimella, and T. F. Fuller, "A critical review of thermal issues in lithium-ion batteries," *Journal of the Electrochemical Society*, vol. 158, no. 3, pp. R1–R25, 2011.

[4] S. G. Lu, Q. T. Shi, and H. B. Tang, "Mathematical analysis and numerical simulation for thermo-stress in a square lithium-ion battery," *Journal of Automotive Safety and Energy*, vol. 5, no. 3, pp. 298–303, 2014.

[5] P. K. Koorata and S. Panchal, "Thermal management of large-sized $LiFePO_4$ pouch cell using simplified mini-channel cold plates," *Applied Thermal Engineering*, vol. 234, article 121286, 2023.

[6] S. Vashisht, D. Rakshit, S. Panchal, M. Fowler, and R. Fraser, "Thermal behaviour of Li-ion battery: an improved electro-thermal model considering the effects of depth of discharge and temperature," *Journal of Energy Storage*, vol. 70, article 107797, 2023.

[7] V. Talele, U. Moralı, M. S. Patil et al., "Computational modelling and statistical evaluation of thermal runaway safety regime response on lithium-ion battery with different cathodic chemistry and varying ambient condition," *International Communications in Heat and Mass Transfer*, vol. 146, p. 106907, 2023.

[8] H. Pegel, D. Wycisk, A. Scheible, L. Tendera, A. Latz, and D. U. Sauer, "Fast-charging performance and optimal thermal management of large-format full-tab cylindrical lithium-ion cells under varying environmental conditions," *Journal of Power Sources*, vol. 556, article 232408, 2023.

[9] A. K. Thakur, R. Sathyamurthy, R. Velraj et al., "A state-of-the art review on advancing battery thermal management systems for fast-charging," *Applied Thermal Engineering*, vol. 226, article 120303, 2023.

[10] L. X. Wu, K. Liu, J. Liu, and H. Pang, "Evaluating the heat generation characteristics of cylindrical lithium-ion battery considering the discharge rates and N/P ratio," *Journal of Energy Storage*, vol. 64, article 107182, 2023.

[11] Y. W. Tang, L. J. Wu, W. F. Wei et al., "Study of the thermal properties during the cyclic process of lithium ion power batteries using the electrochemical-thermal coupling model," *Applied Thermal Engineering*, vol. 137, no. 1, pp. 11–22, 2018.

[12] V. Srinivasan and C. Y. Wang, "Analysis of electrochemical and thermal behavior of li-ion cells," *Journal of the Electrochemical Society*, vol. 150, no. 1, pp. A98–A106, 2003.

[13] M. Xu, R. Wang, B. Reichman, and X. Wang, "Modeling the effect of two-stage fast charging protocol on thermal behavior and charging energy efficiency of lithium-ion batteries," *Journal of Energy Storage*, vol. 20, no. 1, pp. 298–309, 2018.

[14] J. Zhou, L. Chen, S. Zhang, Y. Zhou, S. Wang, and W. Shen, "Distributed thermal monitoring for large-format li-ion battery under limited sensing," *IEEE Transactions on Transportation Electrification*, p. 1, 2023.

[15] M. J. Lin, Y. H. Suo, G. H. Lai, and J. W. Xiao, "Thermal-mechanical coupling analysis of lithium-ionbatteries considering thermal radiation effect underfast charge," *Journal of Shanghai University (Natural Science Edition)*, vol. 29, no. 3, pp. 450–459, 2023, (in Chinese).

[16] W. X. Mei, H. D. Chen, J. H. Sun, and Q. S. Wang, "The effect of electrode design parameters on battery performance and optimization of electrode thickness based on the electrochemical-thermal coupling model," *Sustainable Energy & Fuels*, vol. 3, no. 1, pp. 148–165, 2019.

[17] H. H. Li, A. Saini, C. Y. Liu et al., "Electrochemical and thermal characteristics of prismatic lithium-ion battery based on a three-dimensional electrochemical-thermal coupled model," *Journal of Energy Storage*, vol. 42, no. 1, pp. 1–16, 2021.

[18] B. Jin, J. Q. Zhang, J. G. Gao, X. Shu, and W. Wang, "Thermal-structural coupling analysis of soft pack power lithium batteries for electric vehicles," *Renewable Energy*, vol. 34, no. 4, pp. 563–567, 2016.

[19] O. Valentin, P. X. Thivel, T. Kareemulla, F. Cadiou, and Y. Bultel, "Modeling of thermo-mechanical stresses in Li-ion battery," *Journal of Energy Storage*, vol. 13, pp. 184–192, 2017.

[20] X. X. Zhang, S. Chumakov, X. B. Li et al., "An electro-chemo-thermo-mechanical coupled three-dimensional computational framework for lithium-ion batteries," *Journal of the Electrochemical Society*, vol. 167, no. 16, article 160542, 2020.

[21] Y. H. Suo and J. Liu, "Thermo-mechanical coupling analysis of a cylindrical lithium-on battery with thermal radiation effect in generalized plane strain condition," *International Journal of Energy Research*, vol. 45, no. 2, pp. 1988–1998, 2021.

[22] H. Z. You, H. F. Dai, C. C. Yu, and X. Z. Wei, "Stress properties and modeling of lithium-ion pouch batteries," *Journal of Tongji University*, vol. 48, no. 2, pp. 231–240, 2020.

[23] S. Tian and J. J. Xiao, "Thermal-mechanical coupling analysis of 18650 Li-ion battery under fast charging condition," *Science Technology and Engineering*, vol. 21, no. 7, pp. 2725–2729, 2021.

[24] M. Doyle, T. F. Fuller, and J. Newman, "Modeling of galvanostatic charge and discharge of the lithium polymer insertion cell," *Journal of the Electrochemical Society*, vol. 140, no. 6, pp. 1526–1533, 1993.

[25] P. Chen, *Thermal-electrochemical modeling of Li-ion battery for electric vehicles application*, Beijing Institute of Technology, 2016.

[26] L. Xu, *Charging technology research of the power lithium battery*, Taiyuan University of Science and Technology, 2014.

[27] J. Qian, "Fast charging-Mas three laws," *Chinese LABAT Man*, vol. 2, pp. 18–24, 1979, (in Chinese).

[28] Y. H. Suo, G. H. Lai, and M. J. Lin, "Thermo-mechanical analysis of lithium-ion batteries with variable reversible heat source," *International Journal of Electrochemical Science*, vol. 17, no. 8, article 220847, 2022.

[29] Y. J. Yu, X. G. Tian, and Q. L. Xiong, "Nonlocal thermoelasticity based on nonlocal heat conduction and nonlocal elasticity," *European Journal of Mechanics-A/Solids*, vol. 60, pp. 238–253, 2016.

[30] Y. Z. Peng, K. Zhang, B. L. Zheng, and Y. Li, "Stress analysis of a cylindrical composition-gradient electrode of lithium-ion battery in generalized plane strain condition," *Acta Physica Sinica*, vol. 65, no. 10, article 100201, 2016.

[31] M. R. Eslami, M. Shakeri, and R. Sedaghati, "Coupled thermoelasticity of an axially symmetric cylindrical shell," *Journal of Thermal Stresses*, vol. 17, no. 1, pp. 115–135, 1994.

[32] H. Hu, P. F. Yu, and Y. H. Suo, "Stress induced by diffusion and local chemical reaction in spherical composition-gradient electrodes," *Acta Mechanica*, vol. 231, no. 7, pp. 2669–2678, 2020.

[33] P. B. Nie, S. W. Zhang, A. H. Ran et al., "Full-cycle electrochemical-thermal coupling analysis for commercial lithium-ion batteries," *Applied Thermal Engineering*, vol. 184, article 116258, 2021.

[34] L. M. Wang, J. Y. Niu, W. Zhao, G. C. Li, and X. L. Zhao, "Study on electrochemical and thermal characteristics of lithium-ion battery using the electrochemical-thermal coupled model," *International Journal of Energy Research*, vol. 43, no. 6, pp. 2086–2107, 2019.

[35] L. G. Guo, *Thermal analysis and cooling optimization of lithium-ion power battery*, Chang'an University, 2016.

[36] R. Mathieu, O. Briat, P. Gyan, and J. M. Vinassa, "Fast charging for electric vehicles applications: numerical optimization of a multi-stage charging protocol for lithium-ion battery and impact on cycle life," *Journal of Energy Storage*, vol. 40, article 102756, 2021.